Proceedings of the CERN-BINP Workshop for Young Scientists in e^+e^- Colliders, Geneva, Switzerland, 22 – 25 August 2016, edited by V. Brancolini ans L. Linssen, CERN Proceedings, Vol. 1/2017, CERN-Proceedings-2017-001 (CERN, Geneva, 2017)

Charged Particle Identification using the Liquid Xenon Calorimeter of the CMD-3 Detector

R.R.Akhmetshin, A.N.Amirkhanov, A.V.Anisenkov, V.M.Aulchenko, V.Sh.Banzarov, N.S.Bashtovoy, A.E.Bondar, A.V.Bragin, S.I.Eidelman, D.A.Epifanov, L.B.Epshteyn, A.L.Erofeev, G.V.Fedotovich, S.E.Gayazov, A.A.Grebenuk, S.S.Gribanov, D.N.Grigoriev, F.V.Ignatov, V.L.Ivanov, S.V.Karpov, V.F.Kazanin, O.A.Kovalenko, A.A.Korobov, A.N.Kozyrev, E.A.Kozyrev, P.P.Krokovny, A.E.Kuzmenko, A.S.Kuzmin, I.B.Logashenko, P.A.Lukin, K.Yu.Mikhailov, V.S.Okhapkin, Yu.N.Pestov, A.S.Popov, G.P.Razuvaev, A.A.Ruban, N.M.Ryskulov, A.E.Ryzhenenkov, V.E.Shebalin, D.N.Shemyakin, B.A.Shwartz, A.L.Sibidanov†, E.P.Solodov, V.M.Titov, A.A.Talyshev, A.I.Vorobiov, Yu.V.Yudin*
Budker Institute of Nuclear Physics, SB RAS, Novosibirsk, 630090, Russia

Abstract

This paper describes a currently being developed procedure of the charged particle identification for the CMD-3 detector, installed at the VEPP-2000 collider. The procedure is based on the application of the boosted decision trees classification method and uses as input variables, among others, the specific energy losses of charged particle in the layers of the liquid Xenon calorimeter. The efficiency of the procedure is demonstrated by an example of the extraction of events of the $e^+e^- \to K^+K^-$ process in the center of mass energy range from 1.8 to 2.0 GeV.

Keywords

Particle identification; specific energy losses; boosted decision trees.

1 Introduction

The electron-positron collider VEPP-2000 [1], installed at the Budker Institute of Nuclear Physics (Novosibirsk, Russia), was operating in 2010-2013 and currently is undergoing the final stage of modernization, which will allow it to reach a luminosity of $10^{32}\mathrm{cm}^{-2}\mathrm{s}^{-1}$ at its maximum center of mass (c.m.) energy of $2\,\mathrm{GeV}$. At the two beam intersection points the SND [2] and CMD-3 [3] particle detectors are installed, the main task of which is the measurement of the exclusive cross sections of the electron-positron annihilation into hadrons. Such measurements are necessary to reduce the uncertainty of the hadronic contribution to the anomalous magnetic moment of muon $a_\mu^{\mathrm{had,\,LO}}$ [4, 5].

The tracking system of the CMD-3 detector consists of a cylindrical drift chamber (DC) and a double-layer cylindrical multiwire proportional Z-chamber, installed inside a superconducting solenoid with 1.0–1.3 T magnetic field (see CMD-3 layout in Fig. 1). Amplitude information from the DC wires is used to measure the specific ionization losses (dE/dx_{DC}) of charged particles. Bismuth germanate crystals of 13.4 X_0 thickness are used in the endcap calorimeter. The barrel calorimeter, placed outside the solenoid, consists of two parts: external (based on CsI crystals of 8.1 X_0 thickness) and internal (based on liquid Xenon (LXe) of 5.4 X_0 thickness) [6].

The LXe calorimeter consists of 14 cylindrical ionization chambers formed by 7 cylindrical cathodes and 8 anodes with a $10.2\,\mathrm{mm}$ gap between them (see Fig. 2). Each anode is divided into 264 rectangular pads (8 along the $z-$axis and 33 in the $r-\phi$ plane), forming so-called "towers" oriented to the beams interaction point (see Fig. 1). Signals from pads within one tower are summed up and this information is used to measure the particle energy deposition. Cathodes are divided into 2112 strips

*Corresponding author.
†University of British Columbia, Vancouver, Canada.

2518-315X– © the Author/s, 2017. Published by CERN under the Creative Common Attribution CC BY 4.0 Licence.

https://doi.org/10.23727/CERN-Proceedings-2017-001.77

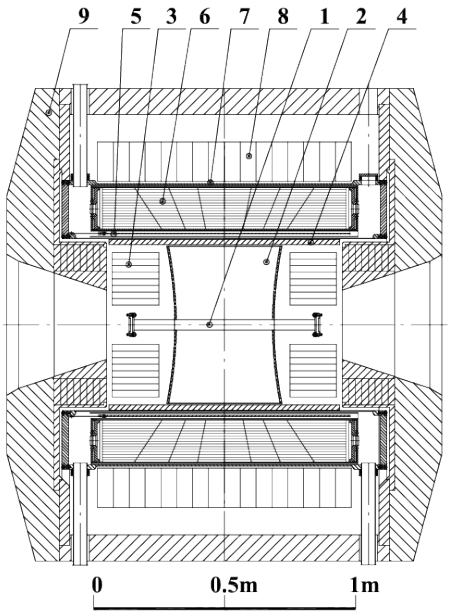

Fig. 1: The CMD-3 detector layout: 1 - beam pipe, 2 - drift chamber, 3 - BGO endcap calorimeter, 4 - Z-chamber, 5 - superconducting solenoid, 6 - LXe calorimeter, 7 - time-of-flight system, 8 - CsI calorimeter, 9 - yoke.

to provide precise coordinate measurement along with the measurement of the specific energy losses ($dE/dx_{\rm LXe}$) in each of 7 double anode-cathode-anode layers (see Fig. 3). Each side of the cathode cylinder contains about 150 strips. The strips on the opposite sides of the cathode are mutually perpendicular, which allows one to measure z and ϕ coordinates of the "hit" in the strips channels. The total amount of material in front of the LXe calorimeter is 0.13 X_0, which includes the solenoid, the radiation shield and vacuum vessel walls.

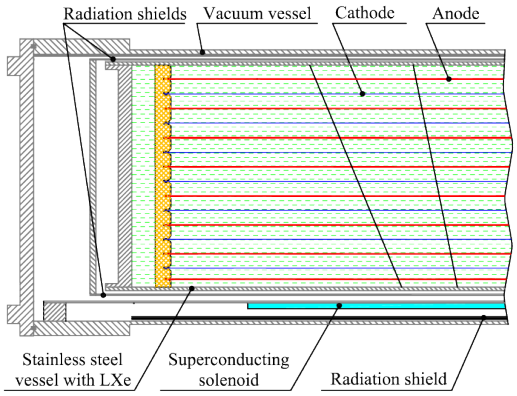

Fig. 2: LXe calorimeter electrodes structure.

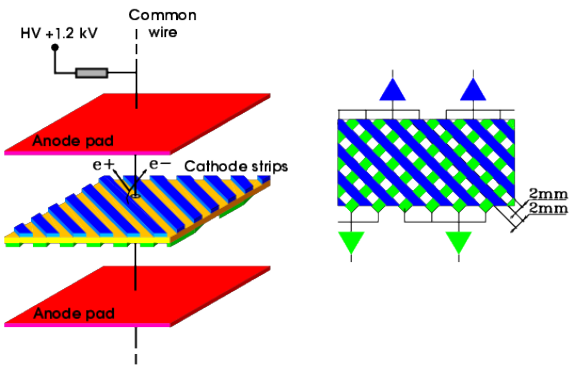

Fig. 3: Anode-cathode-anode layer of the LXe calorimeter. A strip structure of cathode is shown.

For a more accurate measurement of the exclusive cross sections one has to extract a sufficiently background-free sample of the events of the studied process, which requires the development of the effective particle identification (PID) procedure. This paper describes a currently being developed procedure of the charged PID for the CMD-3 detector, which involves the $dE/dx_{\rm DC}$ and $dE/dx_{\rm LXe}$, as well as the energy depositions of charged particles in the LXe ($E_{\rm LXe}$) and CsI ($E_{\rm CsI}$) calorimeters. The efficiency of the procedure is demonstrated by an example of the extraction of the events of the $e^+e^-\to K^+K^-$ process in the c.m. energy range from 1.8 to 2.0 GeV.

2 Charged particle identification with the use of dE/dx_{LXe}

In this paper we will focus on the issue of identification of charged kaons. The separation of the *single* kaons from pions or muons using only dE/dx_{DC} can be reliably performed only for particle momenta lower than $450\,\mathrm{MeV/c}$. This is seen from Figure 4, which shows the distribution of dE/dx_{DC} versus particle momentum for the events of the final state $K^+K^-\pi^+\pi^-$, selected in the experiment [7]. With the use of the energy-momentum conservation law, in the case of this final state a reliable K/π-separation can be performed even up to momenta $700\,\mathrm{MeV/c}$. But for the final states K^+K^-, $K^+K^-\pi^0$, $K^+K^-\pi^0\pi^0$ at high c.m. energies it is hard or impossible to obtain a sufficiently background-free sample of signal events using only dE/dx_{DC} and the energy-momentum conservation law. Hence the dE/dx_{LXe} should be used for PID purposes.

2.1 Binding of the tracks in the DC and LXe

Since the tracks in the DC (DC-tracks) and LXe calorimeter (LXe-tracks) are reconstructed independently, their mutual connection is required. From the kinematics of spiral motion one can derive the rotation angle ϕ_{rot} of the DC-track in the magnetic field B of the solenoid, the expected LXe-cluster polar angle $\theta_{\mathrm{LXe,exp}}$ (measured relative to the central point of the detector) and the penetration angle α_{pen} of the particle to the LXe (the angle between the particle velocity vector and the tangent plane to the surface of the calorimeter at the entry point of the particle):

$$\phi_{\mathrm{rot}} = sign(q) arcsin\left(\frac{1.515{\cdot}R_{\mathrm{LXe}}[\mathrm{cm}]{\cdot}B[\mathrm{T}]}{p_{\perp}[\mathrm{MeV/c}]}\right), \tag{1}$$

$$\theta_{\mathrm{LXe,\,exp}} = arctg\left(\frac{R_{\mathrm{LXe}}}{|z_{\mathrm{DC}} + 2R_{\mathrm{curv}} ctg(\theta_{\mathrm{DC}}) arcsin\left(\frac{R_{\mathrm{LXe}}}{2R_{\mathrm{curv}}}\right)|}\right) + \pi(1 - sign(z_{\mathrm{DC}} + 2R_{\mathrm{curv}} ctg(\theta_{\mathrm{DC}}) arcsin\left(\frac{R_{\mathrm{LXe}}}{2R_{\mathrm{curv}}}\right))), \tag{2}$$

$$\alpha_{\mathrm{pen}} = arcsin\left(sin(\theta_{\mathrm{DC}})\sqrt{1 - \left(\frac{R_{\mathrm{LXe}}}{2R_{\mathrm{curv}}}\right)^2}\right), \tag{3}$$

where q is the particle charge, $R_{\mathrm{LXe}} = 38\,\mathrm{cm}$ the radius of the first cathode cylinder, $p_{\perp}$ the transverse particle momentum, z_{DC} is the z-coordinate of the point of the particle origin (lying on the axis of the beams), θ_{DC} the polar angle of the DC-track, R_{curv} the curvature radius of the DC-track in the $r-\phi$ plane. To bind the DC and LXe tracks we apply the following conditions:

$$|\delta\phi| \equiv |\phi_{\mathrm{LXe,\,meas}} - \phi_{\mathrm{DC}} + \phi_{\mathrm{rot}}| < 0.03\,\mathrm{rad}, \tag{4}$$

$$|\delta\theta| \equiv |\theta_{\mathrm{LXe,\,meas}} - \theta_{\mathrm{DC,\,exp}}| < 0.03\,\mathrm{rad}, \tag{5}$$

where ϕ_{DC} is the azimuthal angle of the departure of DC-track from the beams interaction region, $\phi_{\mathrm{LXe,\,meas}}$ and $\theta_{\mathrm{LXe,\,meas}}$ the measured azimuthal and polar angle of the first strips hit, associated with a reconstructed LXe-track. The $|\delta\phi|$ vs $|\delta\theta|$ distribution in the simulation is shown in Figure 5. It is seen that the mutual connection of the tracks can be performed with a precision of about $0.02\,\mathrm{rad}$ for both azimuthal and polar angles.

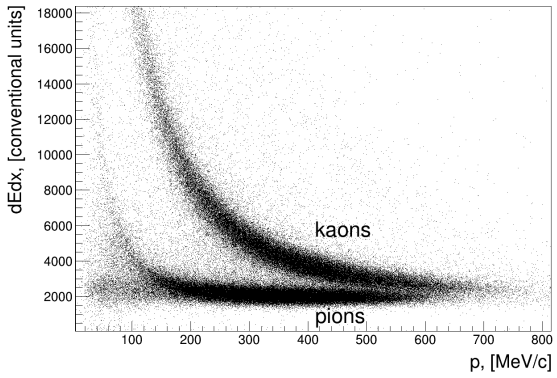

Fig. 4: The $dE/dx_{\rm DC}$ versus particle momentum distribution for the events of the process $K^+K^-\pi^+\pi^-$, selected in the experiment. All energy points from the reaction threshold up to 2 GeV are combined.

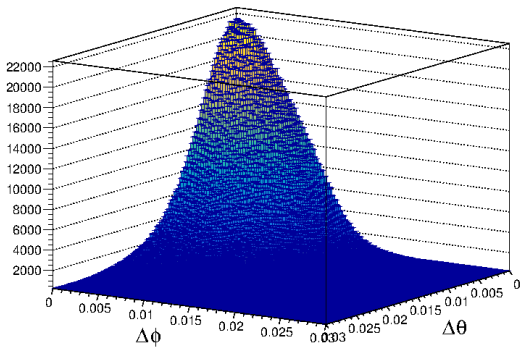

Fig. 5: The $|\delta\phi|$ vs $|\delta\theta|$ parameters distribution for the simulated charged kaons with the momenta, uniformly distributed from 0.04 to 1.0 GeV/c.

2.2 $dE/dx_{\rm LXe}$ vs $dE/dx_{\rm DC}$: general considerations

Distributions of the $dE/dx_{\rm LXe}$ in seven LXe double layers depending on the particle momentum in the DC for the simulated single electrons, muons, charged pions and kaons are shown in Figs 6–7. The following are the most important DC-LXe differences:

- since the particle is inhibited in the layers of calorimeter, $dE/dx_{\rm LXe}$ on average increases layer by layer (see Fig. 8);
- due to dead material in front of LXe calorimeter, and since the procedure of LXe-track reconstruction requires at least 4 strips "hits", there are different momentum thresholds $p_{\rm thr}$ for (anti)protons, kaons, pions, muons and electrons, below which the track in the LXe does not exist or cannot be reconstructed (e.g. for kaons $p^K_{\rm thr}$~$300-350\,{\rm MeV/c}$ (see Fig. 6));
- the values of $p_{\rm thr}$, as well as the distributions of $dE/dx_{\rm LXe}$ in each layer, depend on the parameter $d = 1/sin(\alpha_{\rm pen})$, which characterizes the dependence of the distance passed by the particle in the dead matter and liquid Xenon on the penetration angle $\alpha_{\rm pen}$ of the particle to the LXe;
- in the LXe the kaon and pion interactions with nuclei play important roles. Since the simulation of such interactions can be unreliable, the careful study of the Monte Carlo-experiment differences is required.

2.3 General idea of the particle identification procedure

The idea of the particle identification procedure presented here is the following: for each DC-track, for which the corresponding LXe-track was found, one calculates 10 values of the responses $Resp$ of some multivariate classifier (taken from TMVA package [8]), trained for the separation of the corresponding pairs of particles in the particular momentum p and d parameter ranges δp_i and δd_j (see Table 1). For the training of the classifiers we simulate $4{\cdot}10^6$ events with single $e^{\pm}$, $\mu^{\pm}$, $\pi^{\pm}$, $K^{\pm}$, $p^{\pm}$, having the momentum and d parameter uniformly distributed in the ranges from $0.04\,{\rm GeV}$ to $1.1\,{\rm GeV}$ and from 1.0 to 1.4 correspondingly. Currently we use uniform partitions $\delta p_i = 20\,{\rm MeV/c}$ and $\delta d_j = 0.1$ of the whole available ranges of these parameters, having $53{\times}4$ cells in total.

2.4 The most powerful classifier

Since the K/π separation for $450\,{\rm MeV/c} < p < 900\,{\rm MeV/c}$ is very demanding, the most powerful classifier from about 40 classification methods, proposed by the TMVA package is chosen. $4{\cdot}10^4$ simu-

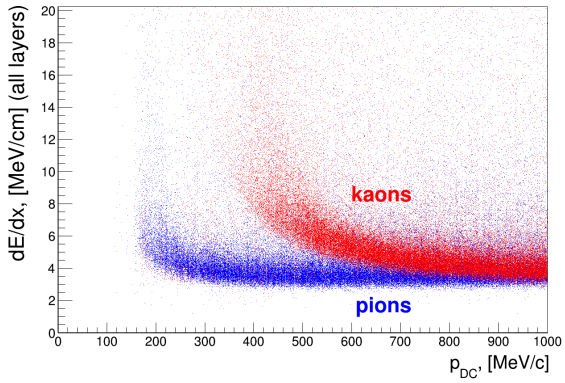

Fig. 6: dE/dx_{LXe} in each of the 7 layers vs particle momentum in the DC for the simulated charged kaons and pions, with the momenta uniformly distributed from 0.04 to 1.0 GeV/c.

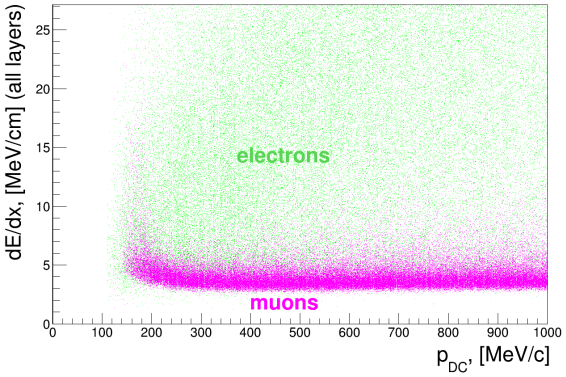

Fig. 7: dE/dx_{LXe} in each of the 7 layers vs particle momentum in the DC for the simulated charged muons and electrons, with the momenta uniformly distributed from 0.04 to 1.0 GeV/c.

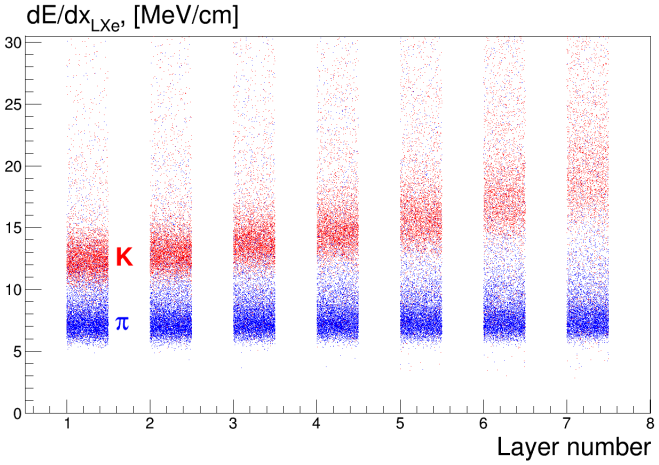

Fig. 8: dE/dx_{LXe} in 7 layers for the simulated charged kaons and pions with the momenta in range from 0.475 to 0.5 GeV/c.

lated kaons and pions are used for training and testing different classifiers, using as the input variables 7 dE/dx_{LXe} values, dE/dx_{DC}, E_{LXe} and E_{CsI}. In Fig. 9 the dependence of the background rejection efficiency on the signal selection efficiency (so-called ROC-curve) is shown for the different classification methods. It is evident, that the globally most powerfull method (at default classifiers settings) is BDT (Boosted Decision Trees). In addition, BDT, compared to different implementations of projective likelihood estimation (PDE) and multi-layer perceptron (MLP), is trained faster. In Fig. 10 one can see the ROC-curves for K/π separation using BDT for different particle momentum ranges from $300\,\mathrm{MeV/c}$ to $900\,\mathrm{MeV/c}$.

2.5 Example: selection of $e^+e^-\to K^+K^-$ events for $\sqrt{s}\in\{1.8\,\mathrm{GeV};2.0\,\mathrm{GeV}\}$

The operation of the described PID procedure can be illustrated by a simple example: the extraction of the events of the $e^+e^-\to K^+K^-$ process in the c.m. energy range from 1.8 to 2.0 GeV. This selection is performed in the experiment on the basis of $11\,\mathrm{pb}^{-1}$ of integrated luminosity, collected by CMD-3 at 18 c.m. energy points in 2011-2012. The events of signal and the major background processes ($e^+e^-\to\pi^+\pi^-$, $\mu^+\mu^-$, e^+e^-) at the same c.m. energy points are simulated.

Table 1: The responses of the multivariate classifiers, trained for the separation of the different pairs of particles in the δp_i and δd_j cell.

	$e^{\pm}$	$\mu^{\pm}$	$\pi^{\pm}$	$K^{\pm}$
$\mu^{\pm}$	$Resp_{i,j}(\mu^{\pm}/e^{\pm})$	-	-	-
$\pi^{\pm}$	$Resp_{i,j}(\pi^{\pm}/e^{\pm})$	$Resp_{i,j}(\pi^{\pm}/\mu^{\pm})$	-	-
$K^{\pm}$	$Resp_{i,j}(K^{\pm}/e^{\pm})$	$Resp_{i,j}(K^{\pm}/\mu^{\pm})$	$Resp_{i,j}(K^{\pm}/\pi^{\pm})$	-
$p^{\pm}$	$Resp_{i,j}(p^{\pm}/e^{\pm})$	$Resp_{i,j}(p^{\pm}/\mu^{\pm})$	$Resp_{i,j}(p^{\pm}/\pi^{\pm})$	$Resp_{i,j}(p^{\pm}/K^{\pm})$

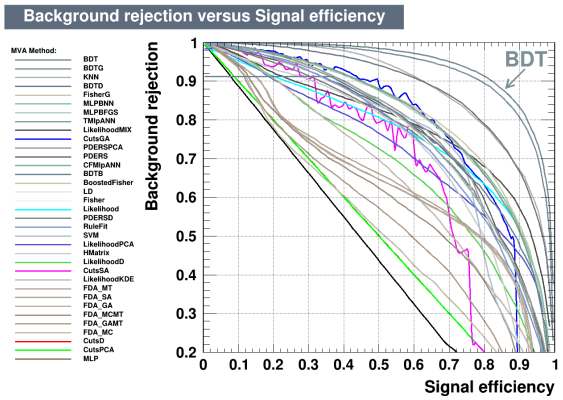

Fig. 9: The ROC-curves for K/π separation at the momenta $870\,\mathrm{MeV/c}$ for different classification methods trained and tested.

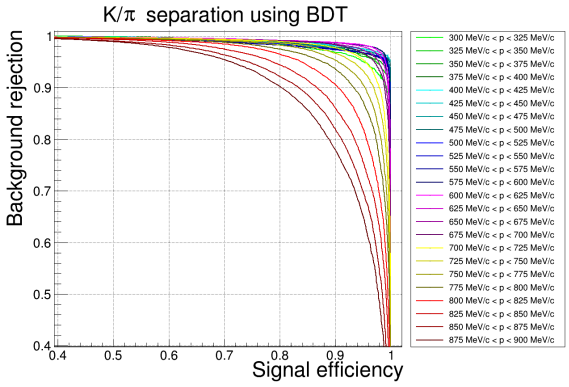

Fig. 10: The BDT ROC-curves for the K/π separation in the different momentum ranges from $300\,\mathrm{MeV/c}$ to $900\,\mathrm{MeV/c}$.

First of all, in the experiment and simulation events having two oppositely charged DC-tracks with polar angles $\theta^{1,2}_{\mathrm{DC}} \in (1.0; \pi - 1.0)$ and satisfying the conditions of collinearity $|\theta^{1}_{\mathrm{DC}} + \theta^{2}_{\mathrm{DC}} - \pi| < 0.25$ and $||\phi^{1}_{\mathrm{DC}} - \phi^{2}_{\mathrm{DC}}| - \pi| < 0.15$ are selected. Further, Figs. 11a–11c show the sum over all c.m. energy point distributions of the average of the positively and negatively charged particles BDT response for the simulated events of signal and the major background processes.

The distribution of the average energy deposition of the charged particles in the calorimeter vs the parameter $\Delta E \equiv \sqrt{\vec{p}^{\,2}_{K^+} + m^2_K} + \sqrt{\vec{p}^{\,2}_{K^-} + m^2_K} - 2E_{\mathrm{beam}}$ in the experiment and simulation is shown in Fig. 12a. In addition to the clusters of K^+K^-, $\pi^+\pi^-$, $\mu^+\mu^-$, e^+e^- final states the horizontal band of cosmic muons is visible. Small dislocations, indicated by arrows, are caused by the tracks passing through the endcap BGO-calorimeter before arriving at the LXe. The long tails to the left of K^+K^- and $\pi^+\pi^-$ clusters are caused by the initial state radiation. To suppress the contribution of the e^+e^- final state, the selection criteria on the averaged BDT response $(\mathrm{BDT}_{K^+/e^+} + \mathrm{BDT}_{K^-/e^-})/2 > 0.2$ (see Fig. 11a) are used. As a result the e^+e^- cluster is almost completely disappeared (see Fig. 12b). Further, to suppress the $\mu^+\mu^-$ background, $(\mathrm{BDT}_{K^+/\mu^+} + \mathrm{BDT}_{K^-/\mu^-})/2 > 0.1$ (see Fig. 11b) is required. As result the contribution of $e^+e^- \to \mu^+\mu^-$ process, as well as the background from the cosmic muons are significantly suppressed (see Fig. 12c). Finally, to suppress the $\pi^+\pi^-$ background $(\mathrm{BDT}_{K^+/\pi^+} + \mathrm{BDT}_{K^-/\pi^-})/2 > 0.05$ (see Fig. 11c) is required, and as a result we obtain an almost background-free sample of K^+K^- events (see Fig. 12d).

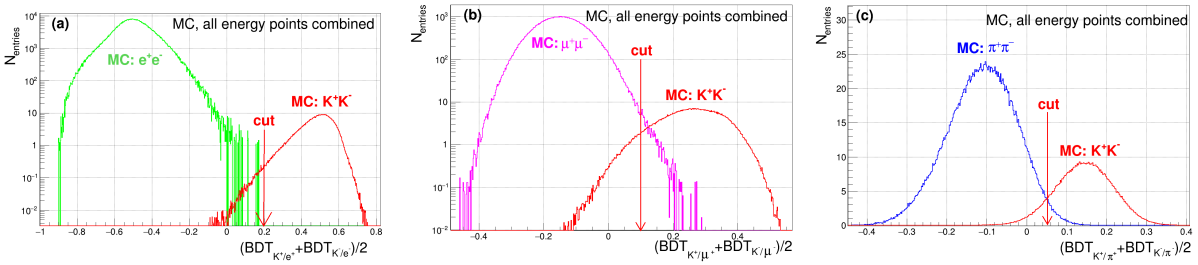

Fig. 11: The distributions of the averaged over the positively and negatively charged particles BDT response for the simulated events of signal and $e^+e^-\to e^+e^-$ (left), $e^+e^-\to\mu^+\mu^-$ (middle), $e^+e^-\to\pi^+\pi^-$ (right) processes. All c.m. energy points are combined. The number of events in each histogram bin is the expected number of events in this bin, in accordance with the luminosity, process cross section and detection efficiency.

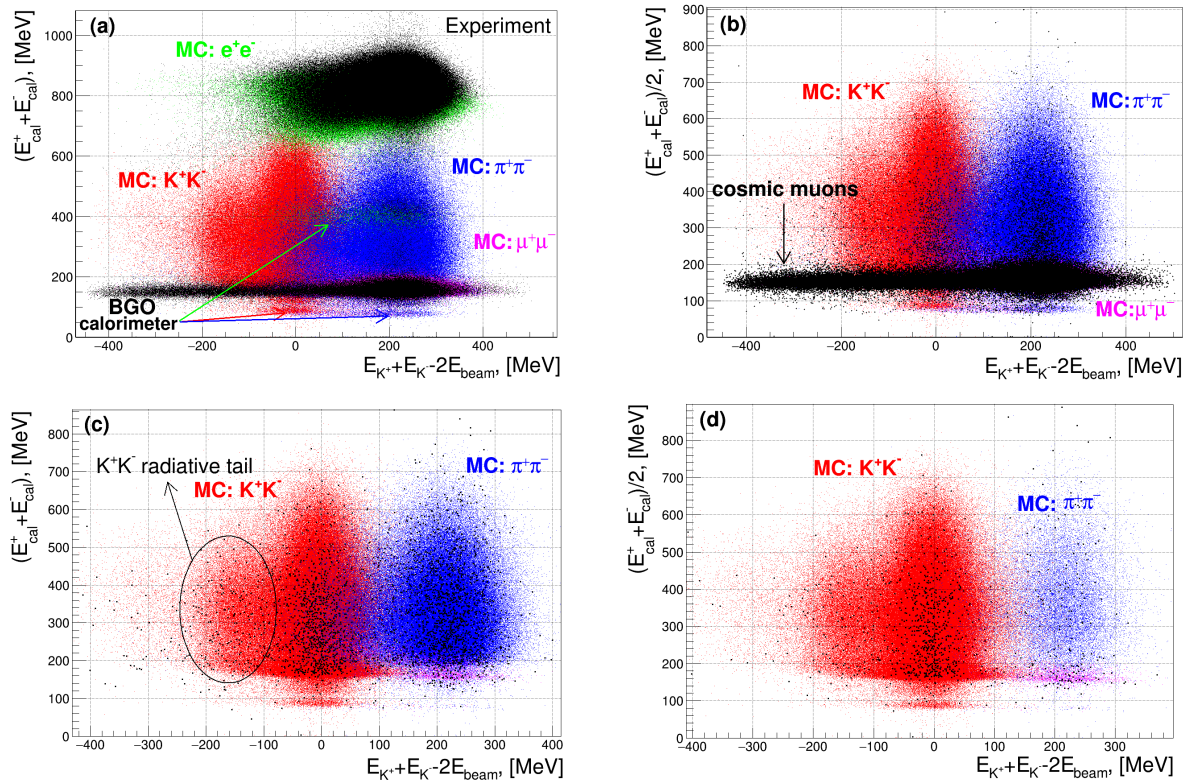

Fig. 12: The distribution of the average energy deposition of the charged particles in the calorimeter vs the ΔE parameter in the experiment and simulation before background suppression (a), after e^+e^- background suppression (b), after e^+e^-, $\mu^+\mu^-$ and cosmic backgrounds suppression (c), after e^+e^-, $\mu^+\mu^-$, cosmic and $\pi^+\pi^-$ backgrounds suppression (d).

3 Plans

Plans for the near future are the following:

1. To allow participation in the PID procedure for the DC-tracks, for which the corresponding LXe-track does not exist or was not reconstructed (which is typical for kaons and (anti)protons at $p < p_{\rm thr}^{K,p^\mp}$);
2. To study the Monte Carlo-experiment differences, especially in the efficiency of LXe-tracks reconstruction:

- for $e^{\pm}$ - on the base of the events of BhaBha scattering;
- for $\mu^{\pm}$ - on the base of cosmic muons;
- for $\pi^{\pm}$ - on the base of a pure $\pi^{\pm}$ sample from the $2\pi^+2\pi^-$ final state;
- for $K^{\pm}$ - on the base of a pure $K^{\pm}$ sample from the $K^+K^-\pi^+\pi^-$ final state;
- for $p^{\pm}$ - on the base of p^+p^- events at low momenta and on the base of protons, ejected from the residual gas at high momenta;

3. To add the response of the muon veto system as a classifier input variable.

4 Conclusion

In this paper the currently being developed charged particle identification procedure for CMD-3 detector was described. The procedure uses, among other input, the information about the specific energy losses of charged particles in the layers of the liquid Xenon calorimeter. Particle identification is based on the responses of 10 multivariate classifiers, trained for the optimal separation of the different types of particles. About 40 different classification methods, provided by TMVA package, were trained and tested, and the most powerful and fast of them was found to be BDT method. The efficiency of the described procedure was demonstrated by an example of the extraction of events of the $e^+e^-\to K^+K^-$ process in the c.m. energy range from 1.8 to 2.0 GeV.

Acknowledgements

We wish to thank the VEPP-2000 personnel for the excellent machine operation. This work is supported in part by the Russian Education and Science Ministry (grant No. 14.610.21.0002, identification number RFMEFI61014X0002), by the Russian Foundation for Basic Research grants RFBR 13-02-00991-a, RFBR 13-02-00215-a, RFBR 12-02-01032-a, RFBR 13-02-01134-a, RFBR14-02-00580-a, RFBR 14-02-31275-mol- a, RFBR 14-02-00047-a, RFBR 14-02-31478-mol-a, RFBR 14-02-91332, RFBR 15-02-05674-a and the DFG grant HA 1457/9-1.

References

[1] I. Koop *et al.*, Nucl. Phys. B, Proc. Suppl. **181**, 371 (2008).

[2] M. N. Achasov *et al.*, Nucl. Instrum. Meth. **A598**, 31 (2009).

[3] B. I. Khazin *et al.*, Nucl. Phys. B, Proc. Suppl. **181-182**, 376 (2008).

[4] K. Hagiwara, R. Liao, A.D. Martin, D. Nomura, T. Teubner, J. Phys. G **38**, 085003 (2011).

[5] M. Davier, A. Hoecker, B. Malaescu, and Z. Zhang, Eur. Phys. J. C **71**, 1515 (2011); Eur. Phys. J. C **72**, 1874 (2012).

[6] V. E. Shebalin *et al.*, JINST **9** no.10, C10013 (2014).

[7] D.N. Shemyakin et al., Phys. Lett. B **756**, 153-160 (2016).

[8] A. Hoecker, P. Speckmayer, J. Stelzer, J. Therhaag, E. von Toerne, and H. Voss, PoS A CAT 040 (2007).